Published in final edited form as:
Nature. 2009 January 1; 457(7225): 92. doi:10.1038/nature07434.

Live-animal tracking of individual haematopoietic stem/progenitor cells in their niche

Cristina Lo Celso[1,4], **Heather E. Fleming**[1,4], **Juwell W. Wu**[3,4], **Cher X. Zhao**[1,4], **Sam Miake-Lye**[1], **Joji Fujisaki**[3,4], **Daniel Côté**[3,†], **David W. Rowe**[5], **Charles P. Lin**[3,4], and **David T. Scadden**[1,2,4,6]

[1]Center for Regenerative Medicine, Massachusetts General Hospital, 185 Cambridge Street, Boston, Massachusetts 02114, USA.

[2]Cancer Center, Massachusetts General Hospital, 185 Cambridge Street, Boston, Massachusetts 02114, USA.

[3]Advanced Microscopy Program, Center for Systems Biology and Wellman Center for Photomedicine, Massachusetts General Hospital, 185 Cambridge Street, Boston, Massachusetts 02114, USA.

[4]Harvard Stem Cell Institute, 42 Church Street, Cambridge, Massachusetts 02138, USA.

[5]University of Connecticut Health Center, 663 Farmington Avenue, Farmington, Connecticut 06030, USA.

[6]Department of Stem Cell and Regenerative Biology, Harvard University, 42 Church Street, Cambridge, Massachusetts 02138, USA.

Abstract

Stem cells reside in a specialized, regulatory environment termed the niche that dictates how they generate, maintain and repair tissues[1,2]. We have previously documented that transplanted haematopoietic stem and progenitor cell populations localize to subdomains of bone-marrow microvessels where the chemokine CXCL12 is particularly abundant[3]. Using a combination of high-resolution confocal microscopy and two-photon video imaging of individual haematopoietic cells in the calvarium bone marrow of living mice over time, we examine the relationship of haematopoietic stem and progenitor cells to blood vessels, osteoblasts and endosteal surface as they home and engraft in irradiated and *c-Kit*-receptor-deficient recipient mice. Osteoblasts were enmeshed in microvessels and relative positioning of stem/progenitor cells within this complex tissue was nonrandom and dynamic. Both cell autonomous and non-autonomous factors influenced primitive cell localization. Different haematopoietic cell subsets localized to distinct locations according to the stage of differentiation. When physiological challenges drove either engraftment or expansion, bone-marrow stem/progenitor cells assumed positions in close proximity to bone and osteoblasts. Our analysis

Correspondence and requests for materials should be addressed to D.T.S. (dscadden@mgh.harvard.edu) or C.P.L. (lin@helix.mgh.harvard.edu).
[†]Present address: Centre de Recherche Université Laval Robert-Giffard, Département de Physique, Université Laval, Québec, Québec G1J 2G3, Canada.

Full Methods and any associated references are available in the online version of the paper at www.nature.com/nature.

Supplementary Information is linked to the online version of the paper at www.nature.com/nature.

The authors declare competing financial interests: details accompany the full-text HTML version of the paper at www.nature.com/nature.

permits observing in real time, at a single cell level, processes that previously have been studied only by their long-term outcome at the organismal level.

Mammalian stem cell niches have largely been defined based on localization of stem cells, with only limited definition of the heterologous cells within the niche that regulate stem cell function. None of these niches has been examined in a physiological context *in vivo*. The haematopoietic stem cell (HSC) niche has been studied by alteration of bone components that induce a change in stem cell function[4–7] or by immunohistochemistry[8–10]. The former does not precisely define localization and the latter does not define function. Several studies have documented the regulatory role of osteoblasts on HSC fate[4,7,8,11–13]; however, other studies have shown that most immunophenotypically defined HSCs can be observed adjacent to the vasculature in bone marrow[9].

Bone-marrow vasculature includes arteries that penetrate compact bone at regular intervals, arborizing into capillaries that converge into a central sinus[14]. CD31 immunostaining of long bones enabled visualization of this vasculature network adjacent to the endosteal surface, particularly in trabecular regions where HSCs are known to localize (Fig. 1a and data not shown)[7,10].

To gain a detailed, dynamic view of haematopoietic stem and progenitor cell (HSPC) localization we used intravital microscopy, scanning 4 mm × 6 mm of mouse calvarium that included the central sinus and the surrounding bone-marrow cavities[3] (Fig. 1b). HSC frequencies in this region are comparable to long bones by immunophenotype and repopulating ability (Supplementary Fig. 2c, d). Because the thickness of long bones precludes analysis by intravital microscopy, we cannot confirm that our results extend to them, particularly the poorly trabeculated diaphysial regions.

Combined confocal and two-photon microscopy permitted visualization to a depth of ~150 μm or 40–60% of the bone marrow cavity in over 75% of our measurements. Simultaneous detection of bone, osteoblasts, vasculature and labelled HSPCs was achieved by second harmonic generation (SHG) microscopy (see Methods), osteoblast-restricted collagen 1α promoter (Col2.3–GFP) reporter mice[15], non-targeted quantumdots (Qdot 655 or 800) injected immediately before imaging, and flow cytometrically sorted cells stained with the lipophilic cyanine dyes Vybrant DiD (1,1′-dioctadecil-3,3,3′-tetramethylindodicarbocyanine perchlorate) or DiI (1,1′-dilinoleyl-3,3,3′, 3′-tetramethylindocarbocyanine perchlorate) (Invitrogen)3, respectively (Fig. 1d–h, Supplementary Fig. 1 and Supplementary Movie 1). Multiple combinations of cell surface markers were used to yield highly enriched long-term reconstituting HSC populations (LT-HSCs) [16,17]. LKS (that is, lineage^{low} (Lin^{low}), c-Kit (Kit)$^{+}$ and Sca1^{+}) CD34^{-}Flk2^{-}, LKS CD150^{+}CD48^{-} and LKS CD48^{-}Flk2^{-} cells were isolated, and represent partially overlapping populations (Supplementary Fig. 7). Given that all flow cytometric methods of cell isolation can only enrich for HSCs, we will refer to all the populations used as haematopoietic stem/progenitor cells (HSPCs) to account for any potential progenitor cell contamination. The isolated cells were not adversely affected by DiD staining based on competitive and serial reconstitution assays of irradiated hosts (Supplementary Fig. 2a, b). Owing to a lack of reporters reliably marking endogenous HSPCs, transplant models were used to track the interactions of HSPCs with the microanatomy of the calvarium.

Z-stacks and three-dimensional reconstructions revealed that green fluorescent protein (GFP)-positive osteoblasts were large, irregular and relatively flat (thickness ~10 μm) cells discontinuously distributed along the endosteal surface (Fig. 1d–g). Osteoblasts were adjacent or in close proximity to vasculature (>60% within 10 μm and >90% within 20 μm of vasculature) (Fig. 1e). Whereas the middle of the cavity contained vasculature that was not associated with osteoblasts, the endosteal region demonstrated close co-localization of

osteoblasts and vessels, suggesting that osteoblast-associated HSPCs would probably also be susceptible to paracrine influence exerted by vascular/perivascular cells.

The efficiency of three-dimensional *in vivo* imaging of HSPCs was compared with immunohistochemistry by injecting 375,000 to 6×10^6 Lin^{low} DiD-labelled cells and recording the number of cells observed per *in vivo* imaged field or per 20 μm fixed, decalcified frozen section. *In vivo* imaging was consistently more sensitive (Supplementary Fig. 3b). To define the boundaries of our *in vivo* detection system, we performed dilution experiments and noted a linear correlation between the number of DiD^+ imaged cells and the number of LKS $CD34^-Flk2^-$ cells injected (Supplementary Fig. 3c). The numbers of cells detected when injecting $5–15 \times 10^3$ LT-HSC-enriched populations were small (3–15 cells per recipient) but consistent, in keeping with the small fraction of the recipients' total bone marrow represented by calvarium[18] and the inefficiencies of HSPC homing19.

HSPCs were detected in the bone marrow cavity as early as 20 min after injection and were static throughout each 1.5- to 3-h-long imaging session. In agreement with a previous study[20], cells were dispersed across the imaged region (Supplementary Fig. 4). To assess precise anatomical relationships in the niche, we acquired *Z*-stack images containing the best focal plane for the DiD signal and the focal plane of the closest endosteal surface (Supplementary Fig. 5). Only HSPCs that were within 60 μm of an endosteal surface were further analysed because beyond that distance we could not distinguish between cells located in the central cavity and those adjacent to deeper endosteum beyond our detection range (see Supplementary Movie 1). This approach excluded only 13% of all imaged cells, mostly detected at depths where SHG, GFP and Qdot signals were too faint to be collected reliably.

We adapted the established lodgement assay[10,21] to observe HSPC localization within the bone marrow of non-irradiated recipients (Fig. 2a). All cells were detected in close proximity to vasculature (0–16 μm) and at variable distances from the endosteum, but never closer than 30 μm (Fig. 2c). Two weeks after injection, we found single, bright, DiD-positive cells located between 15–40 μm from the endosteum (Supplementary Fig. 6a). As expected, no contribution of injected HSPCs to the host peripheral blood or bone marrow was observed for up to 4 months after transplant (data not shown; see also ref. 22). HSPCs injected into non-irradiated hosts localized farther than 30 μm from bone and did not engraft. The lack of engraftment of transplanted HSPCs in physiological niches imposes an inherent limitation on current studies aimed to characterize functional HSCs in their physiological niches *in vivo*.

To visualize HSPCs that could engraft, lethally irradiated wild-type and Col2.3–GFP recipients received HSPC transplants and were imaged 20 min to 5 h after injection. Irradiation compromised the vasculature: the quantum dot fluorescent signal no longer clearly demarcated bone-marrow vessels but instead spilled over the entire cavity (Fig. 2b, red), revealing progressive damage (Fig. 3a, b). Notably, circulating cells followed narrow and well defined trajectories within the quantum dot signal (data not shown), indicating that, after irradiation, bone-marrow vasculature becomes permeable to small particles such as quantum dots but not blood cells.

HSPCs injected into irradiated recipients also localized at variable distances from the endosteum, but under these conditions 47% of the cells were within 15 μm of the endosteal surface (Fig. 2c). We monitored the mice for up to 6 months and observed at least 25% peripheral blood multilineage engraftment in all recipients, thus confirming the functional capacity of the injected cells.

WWv mice carry two mutations in the stem-cell-factor receptor *c-Kit*, resulting in an impaired ability of endogenous HSCs to engage their niche23. As expected, HSPCs injected in non-irradiated WWv mice engraft and overtake endogenous HSC production of all peripheral blood

lineages[23] (Supplementary Fig. 6d). Whereas WWv mice show extramedullary haematopoiesis, secondary bone-marrow transplants confirmed that the injected wild-type HSPCs reside in functional, supportive bone-marrow niches (Supplementary Fig. 6e). Even in the absence of radiation-damaged vasculature, wild-type HSPCs lodged closer to bone surfaces in WWv animals than in wild-type non-irradiated mice (Fig. 2c). Therefore, multiple settings in which donor cells engraft the bone marrow are associated with HSPCs in the bone marrow in close proximity to endosteum.

Engrafting HSCs proliferate within the first 24 h after transplantation [24] and their resulting progeny pass through the multipotent and early progenitor states within 4 days[25], but great heterogeneity in the engraftment features of stem cell populations has been previously reported[26]. Using our system, the *xyz* position of individual cells and their immediate progeny can be tracked *in vivo* over time (Fig. 3a, b), revealing the progressive appearance of cell clusters (Fig. 3c) of decreased dye intensity, consistent with the partitioning of DiD label on cell division (Fig. 3b). To test whether cell clusters arose from an accumulation of migrating cells, we mixed LT-HSC-enriched populations stained with DiD or a second lipophilic dye, DiI, and imaged recipient mice 2 and 3 days after injection. Only a single dye was observed in cells within each cluster (Fig. 3d, e), consistent with the proliferation of single cells associated with early engraftment. Moreover, we observed 5-bromodeoxyuridine (BrdU) uptake by the injected cells using both immunofluorescence and fluorescence-activated cell sorting (FACS) analysis (Supplementary Fig. 9). Our analysis revealed heterogeneity of cell division patterns at the single cell level *in vivo*.

We sought to determine whether positioning within the bone--marrow microenvironment was influenced by intrinsic features of the haematopoietic cells such as differentiation state. We imaged LT-HSC-enriched (LKS $CD34^{-}Flk2^{-}$), multipotent-progenitor-enriched (MPP; LKS $CD34^{+}Flk2^{+}$)[27,28] and committed-progenitor-enriched ($Lin^{low}Kit^{+}Sca^{-}$) populations and the heterogeneous Lin^{low} cells within hours after transplantation (Fig. 4a, b). LT-HSC-enriched cells localized closest to endosteum and osteoblasts, with more mature subsets residing progressively farther away. To determine whether cell position correlated with cell division, we compared the position of cells that had proliferated creating clusters of ≥3 cells with those that did not divide. The quiescent cells were significantly closer to osteoblasts (Fig. 4d).

To determine whether niche variables could influence HSPC localization, we injected cells in wild-type or PPR mice (that is, mice transgenic for a constitutively active parathyroid hormone/parathyroid hormone related peptide receptor driven by the osteoblast specific promoter, *Col12.3kb*)[29]. PPR mice have increased osteoblast number, trabecular bone volume and HSCs[4], and have been shown to drive expansion of injected HSCs when recipients of bone-marrow transplantation[30]. Two days after injection, DiD^{+} cells in PPR mice were markedly closer to the endosteum even when correcting for the reduced bone-marrow cavity size (Fig. 4e and data not shown). Therefore, stem cell non-autonomous features of the niche contribute to the regulation of HSPC localization.

The data presented here demonstrate that the previously proposed dichotomy between distinct osteoblast and perivascular niches is not anatomically feasible in the calvarium: osteoblasts are perivascular. We cannot exclude perivascular-only niches within the diaphysis of long bones or in non-bony tissues such as spleen; however, the microarchitecture of trabeculae indicates a joint periendosteal–perivascular niche. The relationship of transplanted primitive haematopoietic cells to anatomical components of the trabecular niche is influenced by cell-intrinsic and niche-intrinsic variables. Cells of differing immunophenotype localized differently, with closer proximity to bone corresponding to a greater enrichment for stem cell function. In addition, conditions in the microenvironment that enable stem cell engraftment or in which osteoblasts drive HSC expansion yield closer association of HSPCs with bone. There

is anatomical dynamism within the bone marrow, with cell positioning reflecting differing physiological demands on stem cells. However, we cannot conclude that HSPC engraftment or expansion require direct osteoblast contact, as this was not uniformly observed. Rather, approximate vicinity may be sufficient for osteoblast alteration of stem cell function. Gradients of secreted factors and extracellular matrix, or events induced in other surrounding cell types, may contribute to the regulatory function of osteoblasts in the niche.

We have visualized single transplanted HSPCs in their niche within a living mammal and demonstrated that the state of both haematopoietic cell and microenvironment affects the physical association between components of haematopoietic tissue. Continued technical developments and the generation of more sophisticated molecularly modified animal models will permit further analysis of physiologically relevant settings—other than transplantation or artificially permissive environments—and of other stem cells of normal and malignant types as they engage and perhaps compete for niche elements. The combination of molecular, cellular and organismal biology may thereby be simultaneously examined to understand the regulatory networks affecting stem cell control.

METHODS SUMMARY

All mice were housed according to IACUC guidelines and used for experiment when 8–14-weeks old. Wild-type C57BL/6.SJL mice were HSPC donors when recipients were wild type, Col2.3–GFP or WWv double mutant (backcrossed to C57BL/6 background). FVB mice were donors for wild-type or PPR littermate mice4·29 (gift from E. Schipani).

Mice were anaesthetized and prepared for *in vivo* imaging as described[3]. Immediately before imaging 20 μl of non-targeted Qdot 800 or 655 (Invitrogen) diluted in 130 μl sterile PBS was injected retro-orbitally to allow vasculature visualization. The mouse was held in a heated tube mounted on a precision 3 axis motorized stage (Suter MP385). All mice were imaged with a custom-built confocal two-photon hybrid microscope specifically designed for live animal imaging (see Methods). At the start of each imaging session, we surveyed large areas of the skull bone surface using video rate second harmonic microscopy (see Methods) to identify the major anatomical landmarks such as sagittal and coronal sutures. We identified the locations of HSPCs within bone-marrow cavities and recorded their coordinates relative to the intersection of the sagittal and coronal sutures. SHG and GFP signals above each identified HSPC were acquired every 5 to 20 μm until the above endosteal surface was reached. After *in vivo* imaging, the scalp was re-closed using 3 M Vetbond veterinary glue and post-operative care was provided as described[3].

Images were coloured and merged using Adobe Photoshop and HSPC-microenvironment distance measures were obtained using Adobe Illustrator and Microsoft Excel. A two-tailed type 2 *t*-test was applied to all data. *P* values ≤ 0.05 were considered statistically significant.

Supplementary Material

Refer to Web version on PubMed Central for supplementary material.

Acknowledgments

We thank E. Schipani for providing the PPR mice. We are grateful for help and advice from A. Catic, L. Purton, V. Janzen, G. Adams, J. Spencer, J. Runnels and P. O'Donovan. We thank Y. Tang for the mice husbandry care; D. Dombkowski, L. Prickett and K. Folz-Donahue for cell sorting expertise; R. Klein and K. Chomsky-Higgins for technical assistance; and C. Pasker, V. Shannon, M. Indico Miklosik and D. Machon for administrative assistance. C.L.C. was funded by EMBO and HFSP. The project was funded by the National Institutes of Health (to D.T.S. and C.P.L.), the Harvard Stem Cell Institute (to C.P.L.) and philanthropic sources (to D.T.S. and C.L.C.).

References

1. Schofield R. The relationship between the spleen colony-forming cell and the haemopoietic stem cell. Blood Cells 1978;4:7–25. [PubMed: 747780]
2. Xie T, Spradling AC. A niche maintaining germ line stem cells in the *Drosophila* ovary. Science 2000;290:328–330. [PubMed: 11030649]
3. Sipkins DA, et al. *In vivo* imaging of specialized bone marrow endothelial microdomains for tumour engraftment. Nature 2005;435:969–973. [PubMed: 15959517]
4. Calvi LM, et al. Osteoblastic cells regulate the haematopoietic stem cell niche. Nature 2003;425:841–846. [PubMed: 14574413]
5. Nilsson SK, et al. Osteopontin, a key component of the hematopoietic stem cell niche and regulator of primitive hematopoietic progenitor cells. Blood 2005;106:1232–1239. [PubMed: 15845900]
6. Stier S, et al. Osteopontin is a hematopoietic stem cell niche component that negatively regulates stem cell pool size. J. Exp. Med 2005;201:1781–1791. [PubMed: 15928197]
7. Zhang J, et al. Identification of the haematopoietic stem cell niche and control of the niche size. Nature 2003;425:836–841. [PubMed: 14574412]
8. Arai F, et al. Tie2/angiopoietin-1 signaling regulates hematopoietic stem cell quiescence in the bone marrow niche. Cell 2004;118:149–161. [PubMed: 15260986]
9. Kiel MJ, et al. SLAM family receptors distinguish hematopoietic stem and progenitor cells and reveal endothelial niches for stem cells. Cell 2005;121:1109–1121. [PubMed: 15989959]
10. Nilsson SK, Johnston HM, Coverdale JA. Spatial localization of transplanted hemopoietic stem cells: inferences for the localization of stem cell niches. Blood 2001;97:2293–2299. [PubMed: 11290590]
11. Lord BI, Testa NG, Hendry JH. The relative spatial distributions of CFUs and CFUc in the normal mouse femur. Blood 1975;46:65–72. [PubMed: 1131427]
12. Taichman RS, Reilly MJ, Emerson SG. The Hematopoietic microenvironment: Osteoblasts and the hematopoietic microenvironment. Hematology 2000;4:421–426. [PubMed: 11399584]
13. Mayack SR, Wagers AJ. Osteolineage niche cells initiate hematopoietic stem cell mobilization. Blood 2008;112:519–531. [PubMed: 18456874]
14. Crock, HV. The Blood Supply of the Lower Limb Bones in Man. E&S Livingstone LTD; 1967.
15. Kalajzic Z, et al. Directing the expression of a green fluorescent protein transgene in differentiated osteoblasts: comparison between rat type I collagen and rat osteocalcin promoters. Bone 2002;31:654–660. [PubMed: 12531558]
16. Bryder D, Rossi DJ, Weissman IL. Hematopoietic stem cells: the paradigmatic tissue-specific stem cell. Am. J. Pathol 2006;169:338–346. [PubMed: 16877336]
17. Kiel MJ, et al. Haematopoietic stem cells do not asymmetrically segregate chromosomes or retain BrdU. Nature 2007;449:238–242. [PubMed: 17728714]
18. Abkowitz JL, Catlin SN, McCallie MT, Guttorp P. Evidence that the number of hematopoietic stem cells per animal is conserved in mammals. Blood 2002;100:2665–2667. [PubMed: 12239184]
19. Lewin M, et al. Tat peptide-derivatized magnetic nanoparticles allow *in vivo* tracking and recovery of progenitor cells. Nature Biotechnol 2000;18:410–414. [PubMed: 10748521]
20. Suzuki N, et al. Combinatorial Gata2 and Sca1 expression defines hematopoietic stem cells in the bone marrow niche. Proc. Natl Acad. Sci. USA 2006;103:2202–2207. [PubMed: 16461905]
21. Adams GB, et al. Stem cell engraftment at the endosteal niche is specified by the calcium-sensing receptor. Nature 2006;439:599–603. [PubMed: 16382241]
22. Zhong JF, Zhan Y, Anderson WF, Zhao Y. Murine hematopoietic stem cell distribution and proliferation in ablated and nonablated bone marrow transplantation. Blood 2002;100:3521–3526. [PubMed: 12393430]
23. Migliaccio AR, Carta C, Migliaccio G. *In vivo* expansion of purified hematopoietic stem cells transplanted in nonablated W/Wv mice. Exp. Hematol 1999;27:1655–1666. [PubMed: 10560913]
24. Nilsson SK, Dooner MS, Quesenberry PJ. Synchronized cell-cycle induction of engrafting long-term repopulating stem cells. Blood 1997;90:4646–4650. [PubMed: 9373278]

25. Forsberg EC, Serwold T, Kogan S, Weissman IL, Passegue E. New evidence supporting megakaryocyte-erythrocyte potential of flk2/flt3^{+} multipotent hematopoietic progenitors. Cell 2006;126:415–426. [PubMed: 16873070]

26. Dykstra B, et al. Long-term propagation of distinct hematopoietic differentiation programs *in vivo*. Cell Stem Cell 2007;1:218–229. [PubMed: 18371352]

27. Adolfsson J, et al. Identification of Flt3^{+} lympho-myeloid stem cells lacking erythro-megakaryocytic potential: a revised road map for adult blood lineage commitment. Cell 2005;121:295–306. [PubMed: 15851035]

28. Osawa M, Hanada K, Hamada H, Nakauchi H. Long-term lymphohematopoietic reconstitution by a single CD34-low/negative hematopoietic stem cell. Science 1996;273:242–245. [PubMed: 8662508]

29. Calvi LM, et al. Activated parathyroid hormone/parathyroid hormone-related protein receptor in osteoblastic cells differentially affects cortical and trabecular bone. J. Clin. Invest 2001;107:277–286. [PubMed: 11160151]

30. Adams GB, et al. Therapeutic targeting of a stem cell niche. Nature Biotechnol 2007;25:238–243. [PubMed: 17237769]

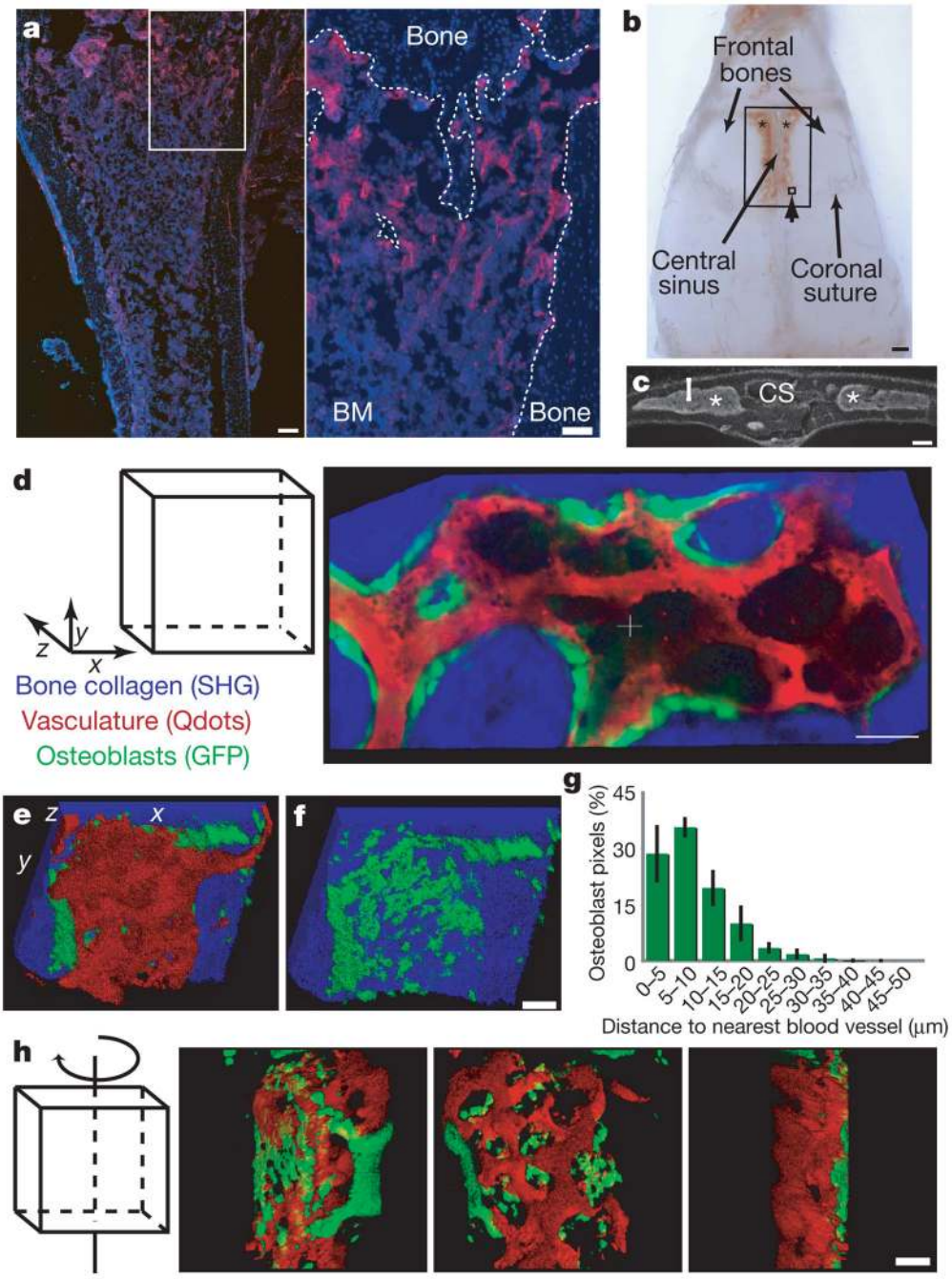

Figure 1. The calvarium endosteal niche is perivascular

a, Anti-CD31 immunofluorescence (red) reveals a complex vascular network in the trabecular region of the tibia and along diaphysis endosteal surface (blue: 4,6-diamidino-2-phenylindole (DAPI) nuclear counter-stain). The right panel shows the boxed area at higher magnification and the dashed line highlights the endosteal surface. Scale bars: left, 200 μm; right, 100 μm. BM, bone marrow. **b**, Intravital microscopy was used to scan the region of mouse calvarium containing bone marrow (asterisks) within the frontal bones. The large box shows the entire scanned area; the small box (arrowhead) shows one approximate observed field (330 μm^2). Scale bar: 1 mm. **c**, DAPI-stained calvarium coronal section indicating cavity morphology (asterisks mark the bone marrow) and depth of scanning (bracket). **d**, *xy* collage image of bone

(blue), osteoblasts (green) and vasculature (red) acquired simultaneously with two-photon microscopy. (See also Supplementary Movie 1.) **e, f**, Three-dimensional reconstructions of *Z*-stack with all three components (**e**) or bone and osteoblasts only (**f**). **g**, Diagram representing measured distance between all osteoblast pixels and the closest vasculature ($n = 4$ cavities; error bars indicate s.d.). **h**, Rotating three-dimensional model of osteoblasts and vasculature. Consistent results were seen with ten mice. Scale bars for **d, f, h** indicate 50 μm.

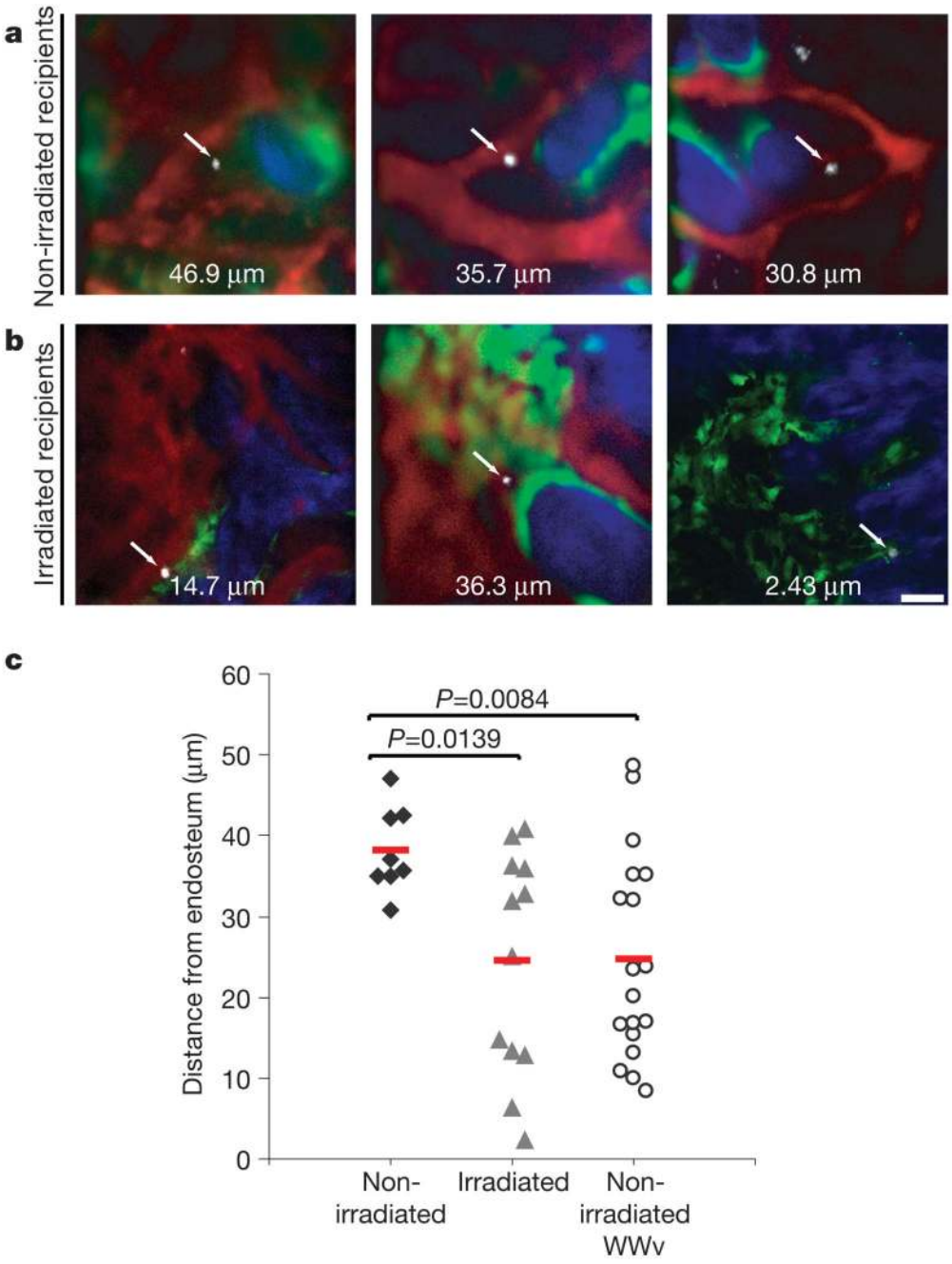

Figure 2. Engrafting HSPCs reach the endosteum

a, b, LKS CD48^{-}Flk2^{-} cells injected into non-irradiated (**a**, $n = 3$ mice) or irradiated recipients (**b**, $n = 3$ mice) were imaged within 5 h of transplantation. Two-photon microscopy was used to detect collagen bone SHG (blue) and confocal microscopy was used to detect DiD signal (white), Qdot vascular dye (red) and GFP-positive osteoblasts (green) in all panels apart from bottom right, where all signals were acquired with two-photon microscopy. Arrows point to single homed HSPCs and the numbers are the *xy* distance measured from each cell to the closest endosteum (edge of blue signal). Scale bar: 50 µm. **c**, The shortest three-dimensional HSPC–endosteal surface distance was plotted for each cell imaged in non-irradiated, irradiated and WWv recipients. The average distance of HSPCs from the endosteum in irradiated and WWv

recipients (n = 3 mice) was significantly less than in non-irradiated recipients. Red lines represent the mean of all measurements for each set of experiments.

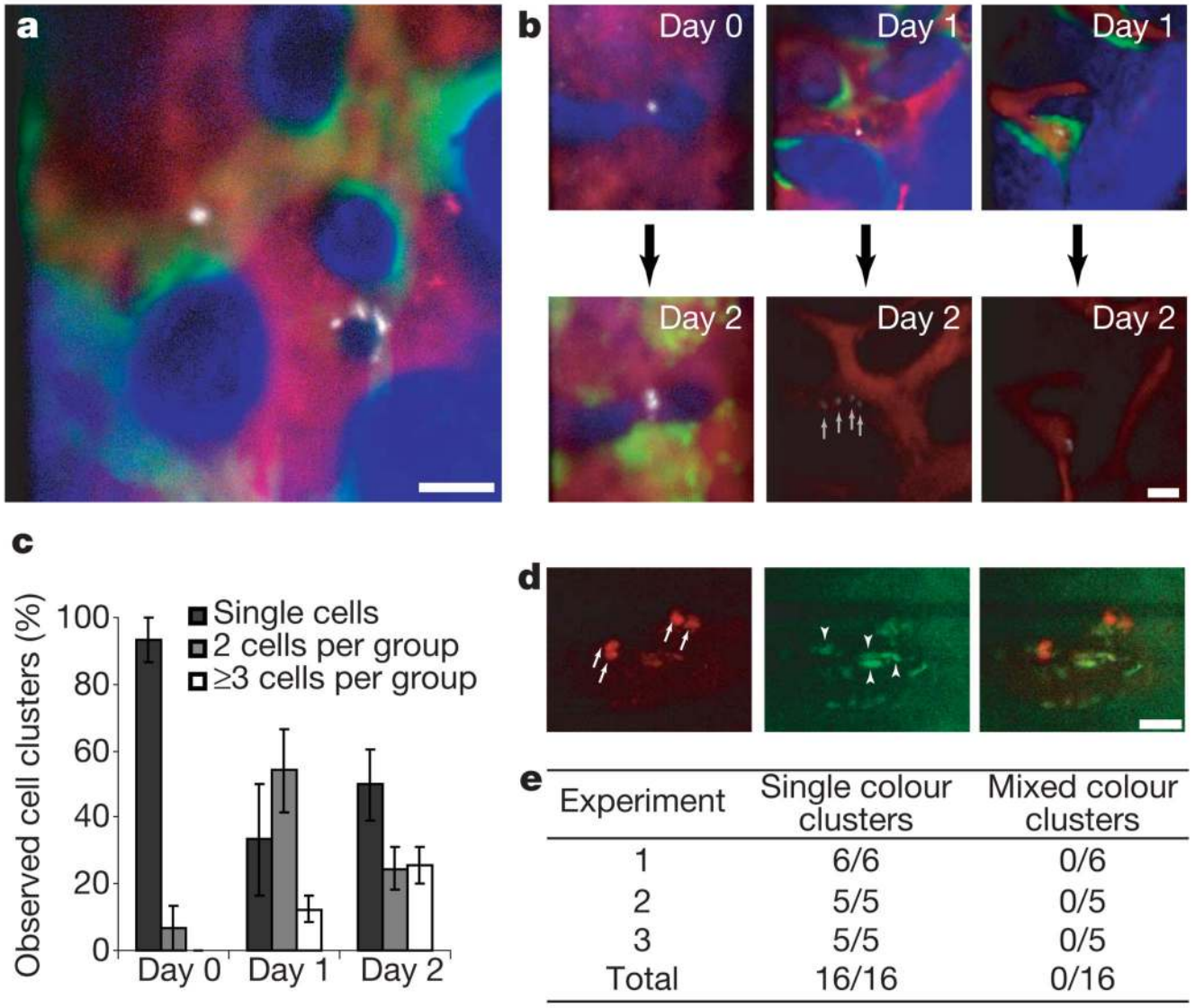

e

Experiment	Single colour clusters	Mixed colour clusters
1	6/6	0/6
2	5/5	0/5
3	5/5	0/5
Total	16/16	0/16

Figure 3. Engraftment is initiated by asynchronous HSPC cell divisions

a, HSPC progeny were imaged 1 day after injection in irradiated recipients ($n = 4$ mice), revealing heterogeneity in cell clustering. Blue, bone; red, vasculature; green, osteoblasts; white, HSPC progeny. **b**, Cells were tracked from day 0 to day 2 ($n = 2$ recipient mice) or from day 1 to day 2 ($n = 3$ recipient mice) and diverse kinetics of cell division were observed. **c**, Increasing numbers of clusters containing 2 or ≥3 cells were observed in the days after injection ($n = 4$; error bars indicate s.e.m.). **d**, When 50% of cells were stained with DiD and 50% with DiI before injection, only single-colour clusters were observed. Red, DiD; green, autofluorescence. Arrows point at each DiD-positive cell within two clusters; arrowheads point at autofluorescent cells. Cells accepted for assessment had a dye/autofluorescence signal ratio >2 (in this example 2.82, 3.71, 4.12, 8.22). The same analysis was used to validate DiI signals. Scale bars in **a, b, d** are 50 μm. **e**, Summary of observed cell clusters in three independent experiments.

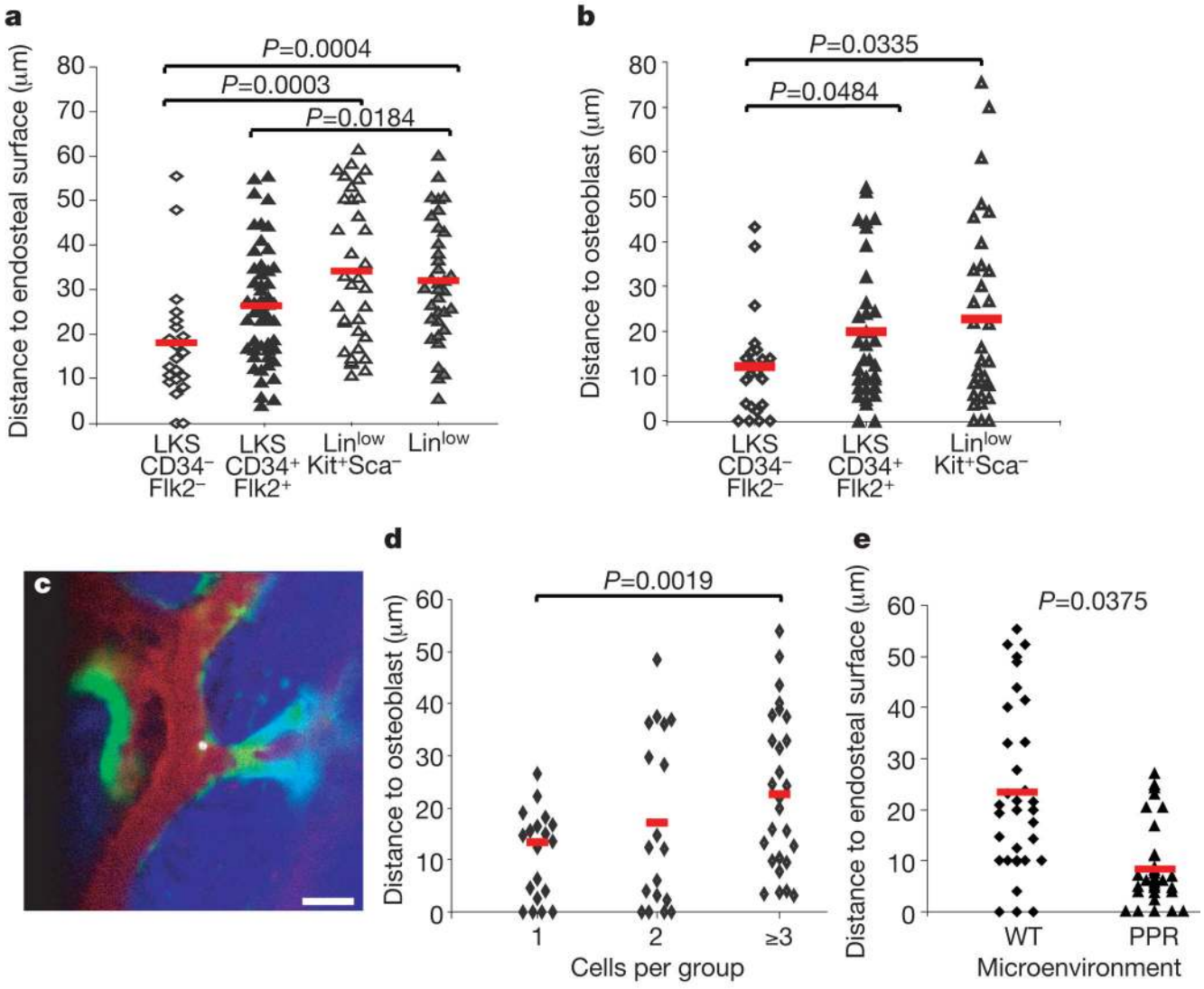

Figure 4. Cell-dependent and niche-dependent HSPC localization

a, b,LKS CD34^{-}Flk2^{-} (n = 6 recipients) LT-HSC-enriched, LKS CD34^{+}FLk2^{+} MPP (n = 3 recipients), Lin^{low}Kit^{+}Sca^{-} progenitors (n = 3 recipients) and Lin^{low} (n = 4 recipients) populations home to distinct locations, closer to or further from endosteum (**a**) and osteoblasts (**b**). All imaging was performed within 5 h of transplantation. **c**, Representative image of a LKS CD34^{-}Flk2^{-} cell residing adjacent to an osteoblast and close to endosteum 4 h after injection. White, DiD-labelled cell; green, GFP^{+} osteoblasts; red, Qdot vascular dye; blue, bone collagen. Scale bar: 50 μm. **d**, Independently of the LT-HSC-enriched starting population, the distance between DiD-labelled cells and osteoblasts measured 2 days after injection increased with the number of cells found in each observed cluster (n = 5 imaged mice). **e**, Two days after injecting the same number of LKS cells in irradiated wild-type or PPR mice (n = 2 + 2) similar numbers of cells were observed, but LKS progeny in PPR mice were preferentially located adjacent to the endosteal surface. Red lines indicate the mean of all measurements in each set of experiments.